Common Spatial Pattern and Wavelet Decomposition for Motor Imagery EEG- fTCD Brain-Computer Interface

Aya Khalaf*, Ervin Sejdic, Murat Akcakaya

Abstract

Background: Recently, hybrid brain-computer interfaces (BCIs) combining more than one modality have been investigated with the aim of boosting the performance of the existing single-modal BCIs in terms of accuracy and information transfer rate (ITR). Previously, we introduced a novel hybrid BCI in which EEG and fTCD modalities are used simultaneously to measure electrical brain activity and cerebral blood velocity during motor imagery (MI) tasks. ***New method:*** In this paper, we used multi-scale analysis and common spatial pattern algorithm to extract EEG and fTCD features. Moreover, we proposed probabilistic fusion of EEG and fTCD evidences instead of concatenating EEG and fTCD feature vectors corresponding to each trial. A Bayesian approach was proposed to fuse EEG and fTCD evidences under 3 different assumptions. ***Results:*** Experimental results showed that 93.85%, 93.71%, and 100% average accuracies and 19.89, 26.55, and 40.83 bits/min average ITRs were achieved for right MI vs baseline, left MI versus baseline, and right MI versus left MI respectively. ***Comparison with existing methods:*** These performance measures outperformed the results we obtained before in our preliminary study in which average accuracies of 88.33%, 89.48%, and 82.38% and average ITRs of 4.17, 5.45, and 10.57 bits/min were achieved for right MI versus baseline, left MI versus baseline, and right MI versus left MI respectively. Moreover, in terms of both accuracy and speed, the EEG- fTCD BCI with the proposed analysis techniques outperformed all EEG- fNIRS studies in comparison. ***Conclusions:*** The proposed system is a more accurate and faster alternative to EEG-fNIRS systems.

***Keywords*—Electroencephalogram, Functional Transcranial Doppler Ultrasound, Hybrid Brain-Computer Interfaces, Common Spatial Pattern, Wavelet Decomposition, Probabilistic Fusion, Support Vector Machines.**

1. Introduction

Brain-computer interfaces (BCIs) exploit brain activity to bypass neuromuscular control with the aim of providing means of control and communication with the surrounding environment for the BCI users [1]. Such systems are of great interest especially for the individuals with neurological deficits causing severe motor impairments [2]. In such cases, BCIs are used mainly for motor

substitution and rehabilitation purposes [3]. In addition, BCIs have other diverse applications in which brain activity is translated into signals that be used for several purposes such as gaming [4], virtual reality [5], and controlling robots [6].

Several acquisition modalities have been employed to measure brain activity using invasive and non-invasive techniques. However, non-invasive modalities are more common in BCI design due to the low risk associated with them compared to invasive modalities [7]. Examples on non-invasive modalities include electroencephalography (EEG) [8], functional magnetic resonance imaging (fMRI) [9], and functional near infrared spectroscopy (fNIRS) [10]. Among non-invasive modalities, EEG is the most common modality used for BCI design due to its high temporal resolution, cost effectiveness, and portability [11]. However, EEG suffers from low signal-to-noise ratio and it encounters non-stationarities due to brain background activities [12]. Moreover, although the performance of EEG-based BCIs is stable in laboratory environment, such performance decreases significantly when the system is used in complex environments or for long periods [13], [14]. BCI performance also decreases when it is controlled by severely motor-impaired patients [15].

In order to overcome the limitations causing the performance decrease of EEG-based BCIs, EEG has been coupled with other control signals that are either brain or non-brain signals [16]. In particular, EEG has been successfully combined with modalities measuring non-brain signals such as signals measured using electromyogram (EMG) and Electrooculography (EOG). For instance, in a hybrid EEG-EOG system, P300, motor imagery (MI), and eye blinking signals have been employed to control wheelchair movement in four different directions [17]. In another study, six different commands generated using both EEG and eye gaze were used for asynchronous wheelchair control [18]. A hybrid EEG-EMG BCI was designed through combining EMG and steady state visually evoked potential (SSVEP) signals. In particular, target stimuli were divided into 4 different groups where EMG was used to infer the group while EEG was used to select the target stimulus within that group [19].

Moreover, EEG was coupled with modalities measuring different brain activities such as fNIRS and fMRI. For instance, a bimodal neurofeedback platform was designed based on simultaneous

acquisition of EEG and fMRI data [20]. In such system, the dimensions of the presented visual task changed based on the feedback from both modalities. For instance, in one of the tasks, a sun was shown on the screen where its brightness was controlled based on EEG feedback while its radius was controlled based on fMRI feedback. In another study, an EEG-fNIRS BCI was designed where EEG was used to detect MI while fNIRS was used to identify MI type [21]. In literature, EEG- fNIRS BCIs are more common compared to EEG-fMRI BCIs since fMRI is non-portable, expensive, and needs a highly controlled environment for efficient performance, therefore, EEG-fMRI BCIs are not suitable for practical applications [22]. However, fNIRS is known to have low-temporal resolution which limit its usage in real-life BCI applications [23]. Moreover, the number of sensors to be used varies depending on the application [24].

Recently, functional transcranial Doppler ultrasound (fTCD) has been used as a faster and cost-effective alternative to fNIRS in BCI design [25], [26]. Therefore, in our previous studies, we suggested using EEG and fTCD for hybrid BCI design [27], [28] . In particular, to find the optimal visual presentation that can maximize the performance of the hybrid EEG-fTCD BCI, two visual presentations were developed and tested. The first visual presentation included MI tasks while the second one included flickering mental rotation (MR) and word generation (WG) tasks. It was found that the proposed MI system outperformed flickering MR/WG system in terms of information transfer rate (ITR) while MR/WG system outperformed MI in terms of accuracy [27], [28].

In this paper, we extend our previous work on MI multimodal hybrid BCI that utilizes EEG and fTCD modalities. In particular, we extend our feature extraction approach by considering features computed based on multiscale analysis and common spatial pattern (CSP) instead of using power spectrum based features we employed previously [27]. It was shown that multiscale analysis captures the changes in fTCD in a timely fashion making it a modality suitable for real-time BCIs [25]. Moreover, CSP is commonly used for EEG-based MI BCIs due to its computational simplicity and ability to find the spatial patterns characteristic to different motor imagery tasks [29]. Using the classical feature extraction approaches described above, we mainly contribute to multi-modal fusion of EEG and fTCD features. In particular, we propose a probabilistic fusion of EEG and fTCD evidences instead of simple concatenation of EEG and fTCD feature vectors. Through such a probabilistic fusion, the contributions of each modality towards the correct

decision can be optimized. More specifically, EEG data was analyzed using common spatial pattern while fTCD data was analyzed using wavelet decomposition. Significant fTCD features were selected using Wilcoxon test. To fuse EEG and fTCD features of each trial, we developed a Bayesian framework and combined EEG and fTCD evidences under 3 different assumptions. Intent inference was made based on maximum likelihood estimation. The proposed analysis technique was used to evaluate 3 binary selection problems including right MI vs baseline, left MI versus baseline, and right MI versus left MI.

2. Materials and Methods

This section includes detailed explanation of data acquisition hardware, presented MI tasks, feature extraction and selection methods as well as feature fusion and classification.

2.1. **Experimental Setup and Data Acquisition**

A total of 10 healthy right-handed participants (6 females and 4 males) were recruited for this study. Before starting the experiment procedures, all participants signed an informed consent. University of Pittsburgh local Institutional Review Board (IRB) approved all procedures employed in this study under IRB number of PRO16080475. Each participant attended one data collection session of 25-min duration and was seated 1-m away from the screen showing the visual presentation presented to each BCI user.

16-electrode *g.tec* EEG system was used for EEG data collection. Electrodes were placed at positions Fp1, Fp2, F3, F4, Fz, Fc1, Fc2, Cz, P1, P2, C1, C2, Cp3, Cp4, P5, and P6. Reference electrode was placed over left mastoid. EEG data was filtered using *g. USBamp*, a bio-signal amplifier, with 8th order bandpass filter of corner frequencies 2 and 62 Hz as well as 4th order notch filter with corner frequencies 58 and 62 Hz.

SONARA TCD system was used for fTCD data collection. In particular, to record fTCD data from left and right middle cerebral arteries (MCAs), two 2 MHz transducers were positioned above the zygomatic arch on the left and right sides of the transtemporal window [30]. MCAs were selected for fTCD data acquisition since they afford approximately 80% of the brain perfusion, therefore, fTCD depth was set to the depth of the mid-point of MCAs (50 mm) [31]. Since fTCD data are

sampled at 44.1 kHz while the fTCD signals are approximately bandlimited to 4.4 kHz, the data were downsampled by a factor of 5 after a low-pass filter with 4.4 kHz corner frequency was applied to avoid antialiasing.

2.2. **Motor Imagery Visual Presentation**

During simultaneous EEG and fTCD data collection, each participant observed visual presentation on which visual icons representing right and left arm MI tasks as well as baseline are constantly shown on the screen. As shown in Fig.1, left horizontal arrow represents left arm MI and right horizontal arrow represents right arm MI while the fixation cross in the middle represents baseline. The task to be performed by the user is randomly selected using a vertical red arrow that keeps pointing to the same task for 10 s which is the trial length. During the visual presentation, 150 trials are presented to the BCI user in a duration of 25 min.

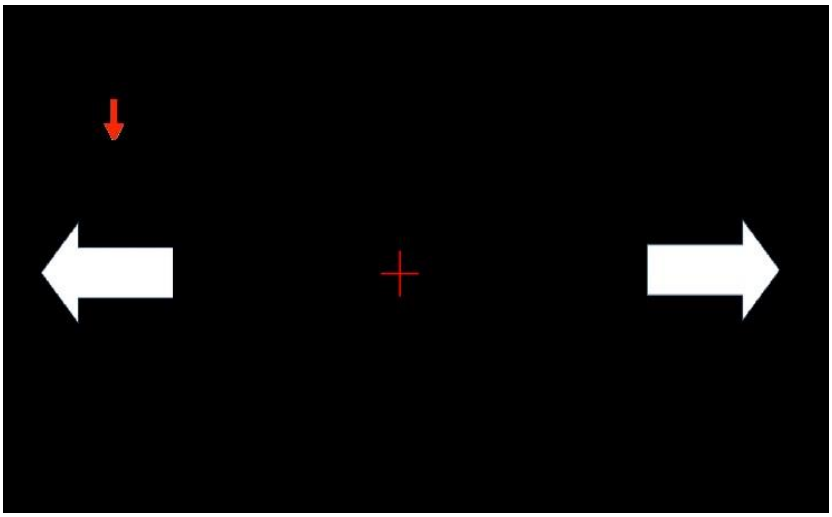

Fig. 1. Stimulus presentation for the hybrid BCI system.

2.3.**Common spatial pattern (CSP)**

In this study, common spatial pattern (CSP) was used to extract features from EEG data. CSP is one of the most efficient feature extraction techniques for MI-based EEG BCIs since characteristic EEG spatial patterns obtained using CSP make MI different tasks significantly differentiable [32]. Basic CSP algorithm is used to analyze multi-channel data based on observations from two classes. In particular, it designs a linear transform that maps the observations from two classes to a new space where they are more discriminative in terms of variance [33]. More specifically, the aim of CSP is to learn the optimal spatial filters which maximize the variance of one class while

minimizing the variance of the other class simultaneously [34]. Finding such spatial filters can be performed through solving the following optimization problem:

$$\max_{W} \; W^{T}\Sigma_{c}W \qquad (1)$$
$$\text{s.t. } W^{T}(\Sigma_{(+)} + \Sigma_{(-)})W = 1$$

where Σ_c is the average trial covariance matrix for class $c \, \epsilon\{+,-\}$ and $w^{T}\Sigma_{c}w$ is the variance in direction w.

Assume each trial is represented by matrix R^{NxT} where N is the number of EEG channels and T is the number of samples. Sample covariance matrix for each trial m is estimated as follows:

$$S_m = \frac{RR^T}{tr(RR^T)} \qquad (2)$$

Average trial covariance matrix can be calculated as follows:

$$\Sigma_{c} = \frac{1}{M}\sum_{m=1}^{M} S_m \qquad (3)$$

Where M is the number of trials belonging to class c.

The optimization problem in (1) can be solved by simultaneous diagonalization of the covariance matrices Σ_c. This can be written as follows:

$$W^{T}\Sigma_{(+)}\,W = \Lambda_{(+)} \qquad (4)$$
$$W^{T}\Sigma_{(-)}W = \Lambda_{(-)}$$
$$\text{s.t. } \Lambda_{(+)} + \Lambda_{(-)} = I$$

Where Λ_c is a diagonal matrix with the eigenvalues λ_j^c , $j = 1,2, \ldots N$ on diagonal.

Solving (4) is equivalent to solving the generalized eigenvalue problem given by:

$$\Sigma_{(+)}w_j = \lambda\Sigma_{(-)}w_j \qquad (5)$$

Where w_j is the j^{th} generalized eigenvector and $\lambda = \frac{\lambda_j^{(+)}}{\lambda_j^{(-)}}$.(4) is satisfied for transformation matrix $W = [w_1 , w_2, \ldots . w_N]$ and λ_j^c given by:

$$\lambda_j^c = w_j^T\Sigma_{c}w_j \qquad (6)$$

Where λ_j^c are the diagonal elements of Λ_c. Given that $\Lambda_{(+)} + \Lambda_{(-)} = I$, consequently, it can be concluded that $\lambda_j^{(+)} + \lambda_j^{(-)} = 1$

For instance, when value of $\lambda_j^{(+)}$ is large, it reflects higher variance in the positive class when filtering it using the spatial filter w_j. In the meantime, a high value of $\lambda_j^{(+)}$yields low value of $\lambda_j^{(-)}$. Therefore, the same spatial filter w_j will result in low variance when used for filtering the negative class. For classification purposes, eigenvectors from both ends of matrix W are considered to maximize the differentiation between the 2 classes. In previous studies [35], [36], [37], it was found that 3 eigenvectors from both ends of W are sufficient to perform the classification task. However, since such choice of the number of eigenvectors used for EEG spatial filtering can vary depending on many parameters such as the number and the location of the electrodes used in each study, in this paper, we solved the 3 binary classification problems at all possible numbers of eigenvectors. In particular, we spatially filtered EEG data using 1, 2, 3, …., and 8 eigenvectors from both ends of W. To extract EEG features, we calculated the log variance of each spatially filtered signal.

2.4. **Wavelet Decomposition**

fTCD data were analyzed using 5-level wavelet decomposition that utilized Daubachies 4 mother wavelet. Such analysis was performed since it was used before with fTCD data and it yielded the most efficient fTCD-based BCI in literature [38]. To reduce the dimensionality of the fTCD feature vector, 4 features were computed for each wavelet band instead of using all wavelet coefficients as features. The 4 features included mean, variance, skewness, and kurtosis. Feature vector corresponding to each trial included 24 features for each channel and 48 features in total.

2.5. **Feature Reduction and Classification**

Wilcoxon signed rank test [39] was used to select the significant features from fTCD feature vectors. p-values of 0.001, 0.005, 0.01, and 0.05 were used. As for EEG, feature vector of each trial contained $2f$ features obtained by projecting the trial data using $f = 1, 2, 3, \ldots$, and 8 eigenvectors from both ends of W. To assess the performance of single-modal BCIs (EEG only and fTCD only BCIs), selected features from each modality were classified solely using support vector machine (SVM) classifier [40]. In particular, performance of fTCD only system was evaluated at p-values of 0.001, 0.005, 0.01, and 0.05. Also, performance of EEG only system was evaluated using $2f$ (2, 4, 6, …., and 16) CSP features. The best set of performance measures for each modality were reported in the results section (Section 3) below.

To evaluate the performance of the hybrid system, EEG feature vector of each trial containing f features was projected into one scalar SVM score (EEG evidence). Moreover, the selected features from the fTCD feature vector were also projected into one scalar SVM score (fTCD evidence). In particular, EEG and fTCD feature vectors corresponding to training trials were used to learn 2 SVM classifiers separately. The 2 classifiers were used to obtain 2 SVM scalar scores representing projected EEG and fTCD feature vectors of each trial under test. EEG and fTCD SVM scores were evaluated at p-values of 0.001, 0.005, 0.01, and 0.05 and $2f$ (2, 4, 6, …., and 16) CSP features. The best set of performance measures were reported in the results section.

2.6. **Bayesian Fusion and Decision Making**

To infer user intent of a given test trial, EEG and fTCD evidences of the training trails were employed in a probabilistic manner. In particular, a Bayesian framework was developed to decide on a test trial under 3 different assumptions. The first assumption ($A1$) assumes EEG and fTCD evidences are jointly distributed while the second assumption ($A2$) assumes evidences of EEG and fTCD are independent. The last assumption ($A3$) assumes EEG and fTCD are independent but they do not have equal contribution towards making a correct decision. To define training and testing sets, the trials of each classification problem were divided into training and testing trials using 10-fold cross validation.

Assume N is the number of trials presented to a certain BCI user. Given a set of EEG and fTCD measurements $\mathrm{Y} = \{\mathrm{y}_1, \ldots \mathrm{y}_N\}$ where $\mathrm{y}_n = \{\mathrm{e}_n, \mathrm{f}_n\}$, e_n and f_n are EEG and fTCD evidences respectively. For a test trial k, the unknown user intent $\mathrm{x_k}$ can be inferred through state estimation using evidences of EEG and fTCD jointly. This is presented in the following optimization problem.

$$\widehat{\mathrm{x_k}} = \arg\max_{\mathrm{x_k}} \mathrm{p}(\mathrm{x_k}|\mathrm{Y} = \mathrm{y}_k) \tag{7}$$

where $\mathrm{p}(\mathrm{x_k}|\mathrm{Y})$ is the state posterior distribution conditioned on the observations Y. Using Bayes rule, (7) can be written as:

$$\widehat{\mathrm{x_k}} = \arg\max_{\mathrm{x_k}} \mathrm{p}(\mathrm{Y} = \mathrm{y}_k|\mathrm{x_k})\ \mathrm{p}(\mathrm{x_k}) \tag{8}$$

where $\mathrm{p}(\mathrm{Y}|\mathrm{x_k})$ is the state conditional distribution of the measurements Y and $\mathrm{p}(\mathrm{x_k})$ is the prior distribution of $\mathrm{x_k}$. This distribution is assumed to be uniform since the trials are randomized. Consequently, (8) can be written as:

$$\widehat{\mathrm{x_k}} = \arg\max_{\mathrm{x_k}} \mathrm{p}(\mathrm{Y} = \mathrm{y}_k|\mathrm{x_k}) \tag{9}$$

Using EEG and fTCD evidences of the training trials, $p(Y|x_k)$ can be computed. To infer user intent at trial k, eqn. (9) can be solved at $Y = y_k$. In this study, the distribution $p(Y|x_k)$ is evaluated under 3 different assumptions as explained in detail below.

2.6.1. **Assumption 1: Joint Distribution**

Given that $y_k = \{e_k, f_k\}$, (9) can be rewritten as:

$$\widehat{x_k} = \arg\max_{x_k} p(e = e_k, f = f_k|x_k) \quad (10)$$

where $p(e, f|x_k)$ is the state conditional joint distribution of EEG and fTCD evidences. Using the EEG and fTCD evidences of N-10 training trials, Kernel density estimation (KDE) with gaussian kernel was performed to find joint distributions $p(e, f|x_k), x_k = 1,2$. To infer user intent at trial k with measurement $y_k = \{e_k, f_k\}$, e_k and f_k are plugged in (10) and the user intent x_k that yields the maximum likelihood is selected.

2.6.2. **Assumption 2: Independent Distributions**

Assuming that the EEG and fTCD evidences, conditioned on the latent state x_k, are independent, accordingly (10) can be written as:

$$\widehat{x_k} = \arg\max_{x_k} p(e = e_k|x_k)p(f = f_k|x_k) \quad (11)$$

where $p(e|x_k)$ and $p(f|x_k)$ are the distributions of EEG and fTCD evidences conditioned on the state x_k respectively. To estimate the distributions $p(e|x_k)$ and $p(f|x_k)$, KDE with gaussian kernel was performed using EEG and fTCD scores of the N-10 training trials. For a trial under test of $y_k = \{e_k, f_k\}$, e_k and f_k are plugged in (11) and the user intent x_k that yields the maximum likelihood is selected.

2.6.3. **Assumption 3: Weighted Independent Distributions**

Here, we propose weighting the conditional distributions $p(e|x_k)$ and $p(f|x_k)$ with weights that sum up to 1 given the fact that the contribution of EEG and fTCD evidences towards making a correct decision might be unequal. Thus (10) can be written as:

$$\widehat{x_k} = \arg\max_{x_k} p(e = e_k|x_k)^{\alpha} p(f = f_k|x_k)^{1-\alpha} \quad (12)$$

where α is a weighting factor that ranges from 0 to 1 with a step of 0.01. $p(e|x_k)$ and $p(f|x_k)$ can be computed as mentioned in section 2.6.2. Such distribution weighting is equivalent to convex combination of the log likelihoods.

For assumption A3, unlike A1 and A2, the training of our hybrid system requires optimizing α value. Such optimization is achieved through grid search over α values ranging from 0 to 1 with a step of 0.01.

2.7. **EEG-fTCD Analysis Across Time**

To evaluate the performance of the hybrid system compared to the single-modal systems (EEG only and fTCD only systems), accuracy and information transfer rate (ITR) [41] were calculated across 10-s period (trial length) for the 3 systems. ITR can be calculated as follows:

$$B = log_2(N) + Plog_2(P) + (1-P)log_2\left(\frac{1-P}{N-1}\right) \quad (13)$$

where P is the classification accuracy, N is the number of BCI classes, and B is the information transfer rate per trial.

Both EEG and fTCD data were analyzed across time at time points 1, 2….,10 *s*. Incremental window with initial length of 1 second and increments of 1 second was used to analyze EEG data while a moving window of 1 second length was used to analyze fTCD data. Moving window was chosen for fTCD analysis based on an fTCD-based BCI study in which performance of both incremental and moving windows was compared [25]. In particular, CSP EEG features and fTCD features at each time window were computed and the performance measures of EEG only and fTCD only systems were calculated at each time point. To compute the performance measures of the hybrid system, EEG and fTCD evidences were combined using the Bayesian framework described in section 2.6 for joint user intent inference. In particular, at each time point (1, 2….,10 *s*), for every trial, EEG and fTCD evidences corresponding to the EEG and fTCD feature vectors at that time point were calculated. Then, these evidences were combined under the 3 different assumptions described in section 2.6 and the corresponding performance measures were calculated.

3. Results

To assess the significance of combining EEG and fTCD for hybrid BCI design, for each participant, maximum possible accuracies obtained using EEG only and fTCD only were compared with maximum accuracy achieved using the hybrid system under the 3 different assumptions (A1, A2, and A3). These accuracies are reported for each individual separately in

Tables 1, 2, and 3 for right MI vs baseline, left MI versus baseline, and right MI vs left MI problems respectively. Moreover, to evaluate the balance of the prediction model, error bars of sensitivities and specificities corresponding to the accuracies reported in Tables 1, 2, and 3 were plotted in Fig.2. In addition, to statistically evaluate the significance of the hybrid combination compared to EEG only, p-values, reported in Table 4 representing the statistical difference between the accuracy vector of A1, A2, and A3 and accuracy vector of EEG only were calculated using Wilcoxon signed rank test. However, statistical comparison in terms of maximum accuracy only is not sufficient to judge the effectiveness of the BCI since accuracy does not reflect the speed of the BCI in contrast to ITR which is a measure that combines both speed and accuracy. Therefore, we compared the hybrid system under A1, A2, and A3 with EEG only and fTCD only in terms of ITRs that are computed at 1 second trial length. We chose 1 second as the trial length because such a selection will enable us to use this system in online applications. Moreover, average ITRs of A1, A2, A3, EEG only, and fTCD only were plotted across the 10-s trial length and presented in Fig. 3.

For right MI versus baseline, Table 1 shows that EEG only achieved average accuracy of 90.52% and fTCD only achieved average accuracy of 64.48% while the hybrid system obtained 91.35%, 92.29%, and 93.85% under A1, A2, and A3 assumptions respectively. Statistical comparisons showed that accuracy vectors of A2 and A3 are significant compared to accuracy vector obtained using EEG only with p-values of 0.002 and 0.0009 while in terms of ITRs, A2 and A3 were found to be significant with p-values 0.0098 and 0.001. For both accuracy and ITR, A1 was found to be insignificant as seen in Tables 4 and 5. As for left MI versus baseline, A1, A2, and A3 obtained average accuracies of 90.72%, 91.96%, and 93.71% respectively while EEG only and fTCD only obtained 92.16% and 61.24% respectively. A1, A2, and A3 were statically compared with accuracy vector due to EEG only. As seen in Table 4, in terms of accuracy, A3 was shown to be statistically insignificant compared to EEG only with a p-value of 0.0625 while A1 and A2 were

TABLE 1

Maximum accuracy achieved for each subject using hybrid combinations (*A1, A2, A3*), EEG only, and fTCD only for right MI vs baseline problem.

Sub_ID	EEG	fTCD	*A1*	*A2*	*A3*
1	92.71%	64.58%	93.75%	93.75%	94.79%
2	90.63%	60.42%	89.58%	90.63%	92.71%
3	81.25%	63.54%	82.29%	82.29%	84.38%
4	87.50%	68.75%	89.58%	93.75%	95.83%
5	96.88%	61.46%	95.83%	97.92%	97.92%
6	86.46%	68.75%	88.54%	89.58%	92.71%
7	93.75%	59.38%	94.79%	94.79%	96.88%
8	95.83%	60.42%	95.83%	96.88%	96.88%
9	87.50%	65.63%	89.58%	89.58%	91.67%
10	92.71%	71.88%	93.75%	93.75%	94.79%
Mean	90.52%	64.48%	91.35%	92.29%	93.85%

TABLE 2

Maximum accuracy achieved for each subject using hybrid combinations (*A1, A2, A3*), EEG only, and fTCD only for left MI vs baseline problem.

Sub_ID	EEG	fTCD	*A1*	*A2*	*A3*
1	92.78%	58.76%	92.78%	91.75%	93.81%
2	93.81%	68.04%	92.78%	92.78%	93.81%
3	91.75%	62.89%	92.78%	94.85%	96.91%
4	87.63%	59.79%	86.60%	83.51%	89.69%
5	92.78%	61.86%	91.75%	89.69%	92.78%
6	87.63%	62.89%	83.51%	93.81%	94.85%
7	93.81%	54.64%	93.81%	94.85%	94.85%
8	95.88%	59.79%	89.69%	90.72%	90.72%
9	91.75%	61.86%	91.75%	93.81%	94.85%
10	93.81%	61.86%	91.75%	93.81%	94.85%
Mean	92.16%	61.24%	90.72%	91.96%	93.71%

TABLE 3

Maximum accuracy achieved for each subject using hybrid combinations (*A1, A2, A3*), EEG only, and fTCD only for right MI vs left MI problem.

Sub_ID	EEG	fTCD	*A1*	*A2*	*A3*
1	93.33%	63.81%	100.00%	100.00%	100.00%
2	88.57%	58.10%	100.00%	100.00%	100.00%
3	92.38%	70.48%	100.00%	100.00%	100.00%
4	91.43%	62.86%	100.00%	100.00%	100.00%
5	93.33%	59.05%	100.00%	100.00%	100.00%
6	90.48%	61.90%	100.00%	100.00%	100.00%
7	96.19%	60.95%	100.00%	100.00%	100.00%
8	100.00%	62.86%	100.00%	100.00%	100.00%
9	95.24%	57.14%	100.00%	100.00%	100.00%
10	80.95%	62.86%	100.00%	100.00%	100.00%
Mean	92.19%	62.00%	100.00%	100.00%	100.00%

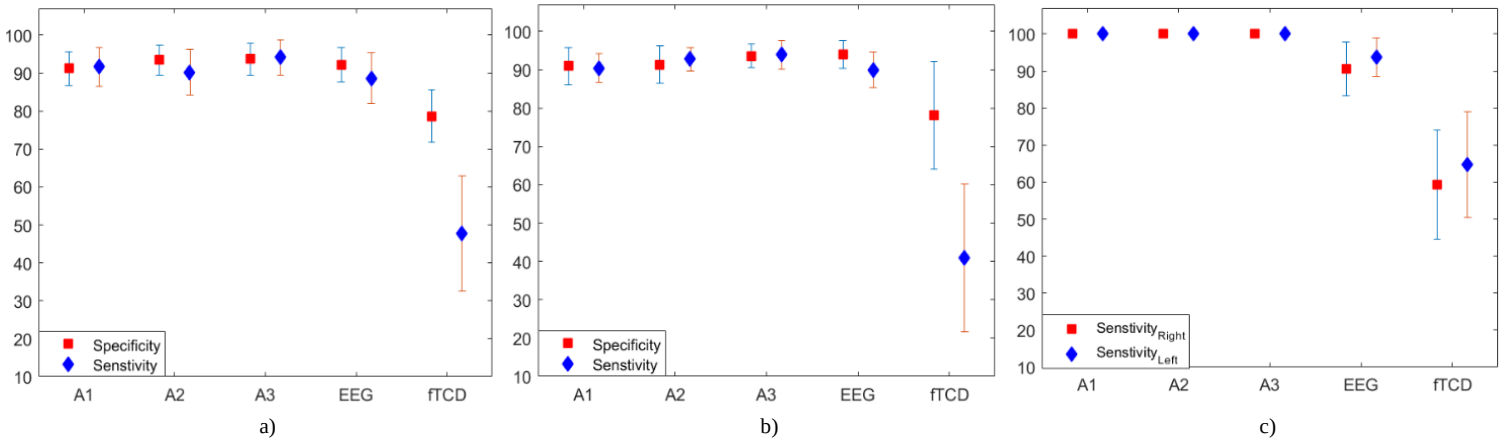

Fig. 2. Sensitivities and specificities (mean and standard deviation) calculated using *A1*, *A2*, *A3*, EEG only, and fTCD only for right MI vs baseline problem (a), left MI vs baseline problem (b), and right MI vs left MI (c).

insignificant compared to EEG only with p-values greater than 0.5. In contrast, in terms of ITR, A3 was found to be significant compared to EEG only with a p-value of 0.001 as shown in Table 5. fTCD average sensitivities and specificities of right MI versus baseline and left MI versus baseline problems were found to be imbalanced as shown in Fig.2. a and Fig.2. b.

As seen in Table 3, the 3 hybrid combinations (A1, A2, and A3) achieved 100% accuracy for right MI versus left MI problem compared to 92.19% and 62.00% obtained using EEG only and fTCD only respectively. In line with these results, p-values of Tables 4 and 5 showed that A1, A2, and A3 are statistically significant compared to EEG only in terms of both accuracy and ITR. Moreover, balanced sensitivities and specificities were achieved using the hybrid system under the 3 assumptions A1, A2, and A3 as well as EEG only and fTCD only as shown in Fig. 2.c.

The results above show that, on average, the accuracy differences between the hybrid system and EEG only are relatively low, however, in terms of ITRs, as seen in Fig.3, average ITRs of A1, A2, and A3 are clearly higher than those achieved using EEG only and fTCD only for the 3 binary selection problems although, according to Table 5, A3 is the only assumption that shows statistical significance for the 3 selection problems when compared to EEG only. In particular, for right MI versus left MI, A1, A2, and A3 achieved maximum ITRs of 39.09, 39.46, and 40.83 bits/min respectively compared to 12.08 and 12.11 bits/min achieved by EEG only and fTCD only. As for right MI versus baseline, A1, A2, A3, EEG only, and fTCD only achieved maximum ITRs of

22.71, 19.89 22.27, 12.08, and 12.11 bits/min respectively. Finally, left MI versus baseline problem yielded maximum ITRs of 10.68 and 17.43 bits/min using EEG only and fTCD only while A1, A2, and A3 obtained 23.87, 24.29, and 26.55 bits/min. In summary, A3 is the only fusion assumption that provided significantly higher performance compared to EEG only system for all the binary selection problems.

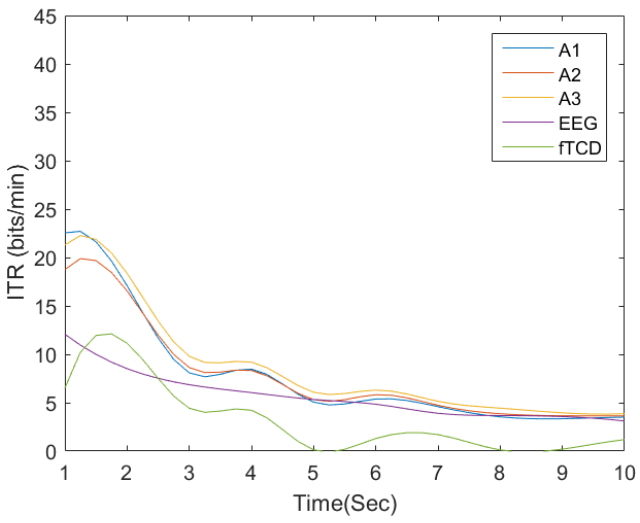

a)

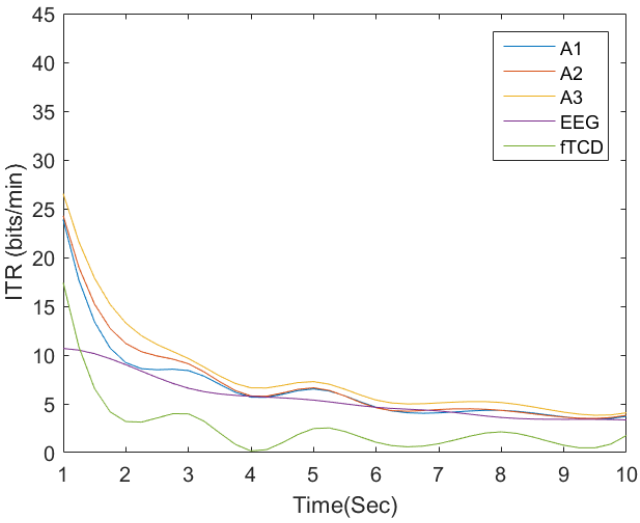

b)

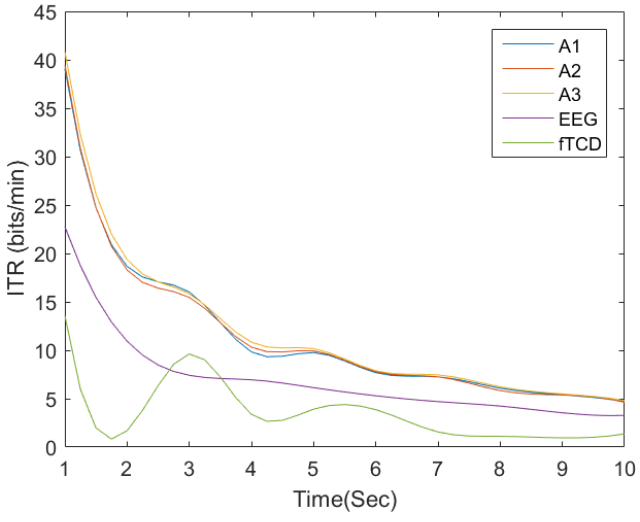

c)

Fig. 3. Average ITRs calculated using EEG only, fTCD only, and the 3 hybrid combinations (*A1*, *A2*, and *A3*) for right MI vs baseline problem (a), left MI vs baseline problem (b), and right MI vs left MI problem (c).

TABLE 4
P-values showing accuracy significance of *A1*, *A2*, and *A3* compared to EEG only for the 3 binary problems.

Comparison	Right MI vs Baseline	Left MI vs Baseline	Right MI vs Left MI
A1/EEG	0.1055	0.9922	0.0020
A2/EEG	0.0020	0.5332	0.0020
A3/EEG	0.0009	0.0625	0.0020

TABLE 5
P-values showing ITR significance of *A1*, *A2*, and *A3* compared to EEG only for the 3 binary problems.

Comparison	Right MI vs Baseline	Left MI vs Baseline	Right MI vs Left MI
A1/EEG	0.0938	0.2461	0.0059
A2/EEG	0.0098	0.1250	0.0029
A3/EEG	0.0010	0.0010	0.0010

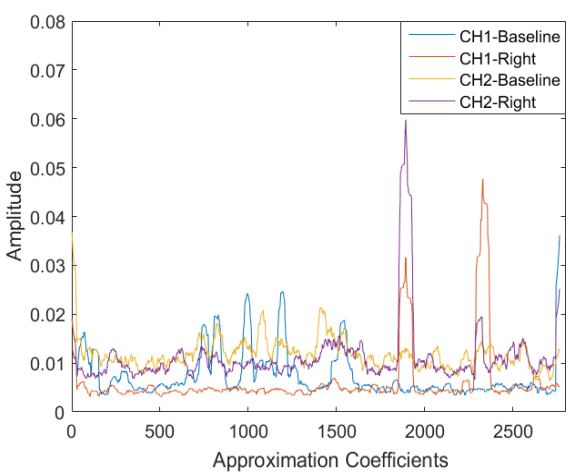

a)

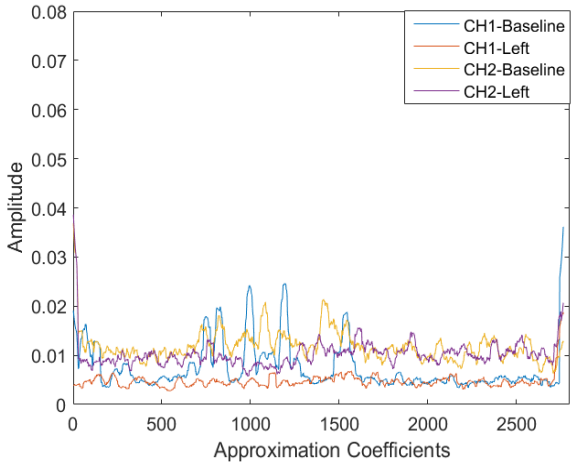

b)

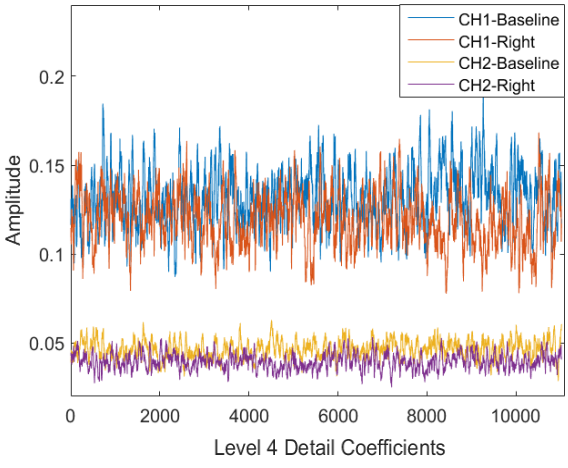

c)

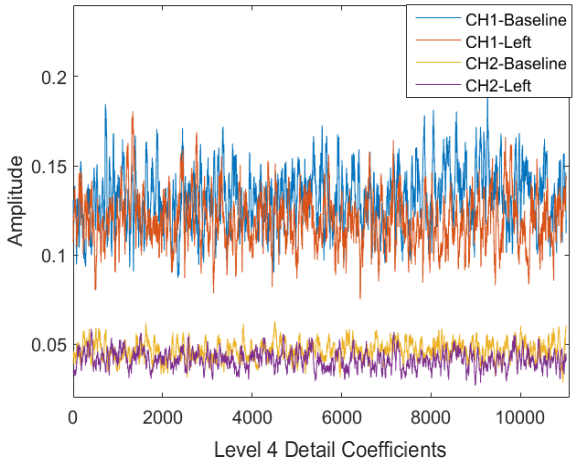

d)

Fig. 4. For each task, wavelet coefficients of each wavelet band were averaged across trials corresponding to that task. The figure shows average approximation and level 4 detail wavelet coefficients for right MI vs baseline problem (a, c) and left MI vs baseline problem (b, d). It can be noted that, for each fTCD channel, the difference between right MI coefficients and baseline coefficients (Fig.4. a and Fig.4. c) is higher than the difference between left MI coefficients and baseline coefficients (Fig.4. b and Fig.4. d).

4. Discussion

In general, it can be noted that the proposed analysis approach including feature extraction and probabilistic fusion stages did not significantly boost the performance of the hybrid system compared to EEG only in terms of accuracy. However, the proposed analysis resulted in average ITR that is 5 times the average ITR obtained previously for right/left MI versus baseline [27]. Moreover, the average ITR of the right MI versus left MI problem is 4 times the ITR achieved before for the same problem [27].

Considering the performance of the hybrid system for the 3 binary selection problems, it was found that right MI versus left MI problem obtained significantly higher average accuracy and average ITR compared to left/right MI versus baseline problems under assumptions A1, A2, and A3. Specifically, 100% accuracy was obtained under the 3 different assumptions compared to 93.85% and 93.71% achieved by right MI versus baseline and left MI versus baseline respectively while average ITRs of 40.83, 19.89, and 26.55 bits/min were obtained for right MI versus left MI, right MI versus baseline, and left MI versus baseline respectively. Such results indicate that the information provided by EEG and fTCD modalities during task versus task problem are well suited to complement each other.

In terms of both accuracy and ITR, as seen in Tables 1, 2, 3,4, and 5, the hybrid system under assumptions A2 and A3 outperformed EEG only for right MI versus baseline and right MI versus left MI problems. For left MI versus baseline problem, although hybrid system under A1, A2, and A3 did not provide significant improvement compared to EEG only in terms of accuracy, the hybrid system under A3 provided a significant improvement in terms of ITRs as shown in Table 5. Considering the 3 binary selection problems, it can be concluded that A3 provides significantly higher accuracies and/or ITRs compared to EEG only as seen in Tables 1-3, Fig. 3, and confirmed by the statistical comparisons shown in Tables 4 and 5. Therefore, we believe that the system can perform efficiently under the weighted independence assumption (A3).

Although the accuracy due to EEG only for left MI versus baseline problem was higher than the EEG accuracy of right MI versus baseline problem, assumptions A2 and A3 failed to significantly

improve the accuracy of the hybrid system compared to EEG only for left MI versus baseline while same assumptions succeeded to significantly improve the hybrid performance for right MI versus baseline compared to EEG only. Therefore, we claim that such failure occurred because fTCD could not boost the performance of the system due to limitations related to the features extracted from fTCD data and how well these features are able to highlight the differences between left MI and baseline. To prove such a claim, at different decomposition levels, we investigated wavelet coefficients from which the fTCD statistical features were derived. As seen in Fig.4, for each fTCD channel, the difference between right MI coefficients and baseline coefficients (Fig.4. a and Fig.4. c) is higher than the difference between left MI coefficients and baseline coefficients (Fig.4. b and Fig.4. d). Moreover, the differences between the wavelet coefficients due to MI tasks and baseline seem to be localized rather than global while the statistical features we extract in this paper are calculated for all coefficients within each wavelet band. For instance, out of around 2700 approximation coefficients, only 500 coefficients highlight the differences between left MI and baseline coefficients as shown in Fig.4. b while many more coefficients highlight the differences between right MI and baseline as seen in Fig.4. a. Considering level 4 detail coefficients, for left MI versus baseline, the differences between the coefficients were more noticeable for the last 3000 coefficients out of 11000 in total for both channels while for right MI versus baseline, the differences were obvious over all the coefficients representing channel 2 and over the last 3000 coefficients representing channel 1.

In general, since the difference between right MI and baseline coefficients is more obvious than the difference between left MI and baseline coefficients, the global features were able to better highlight the differences between right MI and baseline and, therefore, improve the hybrid performance compared to EEG only for right MI versus baseline. Considering Fig.4. a and Fig.4. b, for both channels, it can be noted that the difference between right MI and left MI coefficients is more noticeable than the right MI-baseline difference and left MI-baseline difference. Such observation explains the reason why fTCD provided more significant information for right MI versus left MI problem.

In this paper, extraction of fTCD global statistical features was performed with the aim of reducing the computational complexity of the system through extracting few numbers of features rather than

utilizing the wavelet coefficients themselves as features which will result in a very high-dimentional feature vector. To address local changes in the wavelet coefficients, as one of our future directions, we will calculate localized statistical features for each wavelet band though dividing each band into segments with equal length where the segment length can be determined based on the calibration sessions of each participant.

In our preliminary study in which we introduced MI hybrid EEG-fTCD BCI, average accuracies of 88.33%, 89.48%, and 82.38% and average ITRs of 4.17, 5.45, and 10.57 bits/min were achieved for right MI versus baseline, left MI versus baseline, and right MI versus left MI respectively [27]. In the current study, we succeeded to significantly improve both accuracy and ITR of the proposed MI-based hybrid system. In particular, the current analysis yielded 93.85%, 93.71%, and 100% average accuracy and 19.89, 26.55, and 40.83 bits/min average ITRs for right MI versus baseline, left MI versus baseline, and right MI versus left MI respectively.

Moreover, to evaluate the performance of the 2 visual presentations we designed for the hybrid EEG-fTCD system, we compared the current performance measures obtained using MI visual presentation with the preliminary performance measures we obtained using MR/WG visual presentation [28] As seen in Table 6, MI visual presentation using the current analysis approach outperformed MR/WG visual presentation in terms of accuracy. In terms of ITR, average ITRs obtained using MR/WG visual presentation were 4.39, 3.92, and 5.60 bits/min for MR versus baseline, WG versus baseline, and WG versus MR classification respectively [28]. Such ITRs are significantly lower than the ITRs we obtained in the current study using MI visual presentation especially for task versus baseline problems.

Since the hybrid EEG-fTCD system is suggested as a faster alternative for EEG-fNIRS BCIs, we compared our results with the binary EEG-fNIRS BCIs in literature in terms of accuracy and trial length. As seen in Table 6, the MI EEG-fTCD system with the proposed analysis approach outperforms all the studies in comparison in terms of accuracy for the task versus task problem. For task versus baseline problems, the achieved accuracies are comparable to those obtained in studies [42], [43], [44]. However, unlike the hybrid BCIs in comparison, the proposed system does not require baseline/rest periods before/after each task yielding a total trial length that is shorter

than trial length of all studies in comparison. Therefore, inference of the user intent can be achieved faster using the proposed hybrid system with the current analysis approach.

TABLE 6

Comparison between the proposed hybrid system and the state-of-the-art hybrid BCIs.

Method	Activity	Modalities	Accuracy	Trial length (s)	
				Task	Baseline/rest
[45] Fazli et al., 2012	Motor Imagery	EEG+fNIRS	83.20%	5	6/0
[45] Fazli et al., 2012	Motor Execution	EEG+fNIRS	93.20%	5	6/0
[46] Blokland et al., 2014	Motor Imagery	EEG+fNIRS	79.00%	15	0/30±3
[46] Blokland et al., 2014	Motor Execution	EEG+fNIRS	87.00%	15	0/30±3
[42] Khan et al., 2014	Mental Arithmetic	EEG+fNIRS	83.60%	10	0/5
[42] Khan et al., 2014	Motor Execution	EEG+fNIRS	94.70%	10	0/5
[43] Putze et al., 2014	Visual/auditory stimuli	EEG+fNIRS	94.70%	12.5±2.5	0/20 ±5
[47] Yin et al., 2015	Motor Imagery	EEG+fNIRS	89.00%	10	0/21±1
[21] Koo et al. 2015	Motor Imagery	fTCD+NIRS	88.00%	15	0/60
[44] Buccino et al., 2016	Motor Execution	EEG+fNIRS	72.20%	6	6/0
[44] Buccino et al., 2016	Motor Execution	EEG+fNIRS	94.20%	6	6/0
[48] Shin et al., 2017	Mental Arithmetic	EEG+fNIRS	88.20%	10	0/16±1
[28] Khalaf et al.,2018 (MR/baseline)	SSVEP+ MR/WG	EEG+fTCD	89.11%	10	NA
[28] Khalaf et al.,2018 (WG/baseline)	SSVEP+ MR/WG	EEG+fTCD	80.88%	10	NA
[28] Khalaf et al.,2018 (MR/WG)	SSVEP+ MR/WG	EEG+fTCD	92.38%	10	NA
[27] Khalaf et al.,2019 (right/baseline)	Motor Imagery	EEG+fTCD	88.33%	10	NA
[27] Khalaf et al.,2019 (left/baseline)	Motor Imagery	EEG+fTCD	89.48%	10	NA
[27] Khalaf et al.,2019 (right/left)	Motor Imagery	EEG+fTCD	82.38%	10	NA
Proposed method (right/baseline)	Motor Imagery	EEG+fTCD	**93.85%**	10	NA
Proposed method (left/baseline)	Motor Imagery	EEG+fTCD	**93.71%**	10	NA
Proposed method (right/left)	Motor Imagery	EEG+fTCD	**100.00%**	10	NA

*NA: Not applicable

5. Conclusion

In this paper, through fTCD multiscale analysis and CSP-based EEG analysis, we improved the performance of our novel MI hybrid system in which EEG and fTCD data are acquired simultaneously during visual presentation of MI tasks to the BCI users. Moreover, we proposed a probabilistic fusion approach of EEG and fTCD evidences instead of concatenating EEG and fTCD feature vectors of each trial. The proposed approach fuses EEG and fTCD evidences under 3 different assumptions. To evaluate the performance of the hybrid system compared to single-

modal EEG and fTCD systems, we formulated 3 binary selection problems including right MI versus baseline, left MI versus baseline, and right MI versus left MI. It was found the hybrid system achieves the highest performance under assumption (A3) that assumes that EEG and fTCD are independent, but they do not have equal contribution towards making a correct decision. In particular, the hybrid system achieved average accuracies of 93.85%, 93.71%, and 100% and ITRs of 19.89, 26.55, and 40.83 bits/min for right MI versus baseline, left MI versus baseline, and right MI versus left MI respectively while the same problems yielded 90.52%, 92.16%, and 92.19% average accuracy and ITRs of 12.08, 10.68, and 22.76 bits/min respectively using EEG only. Compared to both hybrid EEG-fNIRS and EEG-fTCD BCIs in literature, the system with the current analysis approach outperformed all the studies in comparison. In addition to these significant results, the proposed system is portable and cost-effective compared to the other multimodal BCIs that exploits multimodal brain activity such as EEG-fMRI, EEG-MEG, and EEG-fNIRS BCIs. Moreover, the proposed system is easier to setup (in terms of number of sensors) and faster (in terms of trial length) compared to hybrid BCIs that utilize EEG and fNIRS simultaneously.

References

[1] L. F. Nicolas-Alonso and J. Gomez-Gil, "Brain computer interfaces, a review.," *Sensors (Basel).*, vol. 12, no. 2, pp. 1211–79, 2012.

[2] I. Lazarou, S. Nikolopoulos, P. C. Petrantonakis, I. Kompatsiaris, and M. Tsolaki, "EEG-Based Brain–Computer Interfaces for Communication and Rehabilitation of People with Motor Impairment: A Novel Approach of the 21st Century," *Front. Hum. Neurosci.*, vol. 12, p. 14, Jan. 2018.

[3] L. E. H. van Dokkum, T. Ward, and I. Laffont, "Brain computer interfaces for neurorehabilitation – its current status as a rehabilitation strategy post-stroke," *Ann. Phys. Rehabil. Med.*, vol. 58, no. 1, pp. 3–8, Feb. 2015.

[4] M. Ahn, M. Lee, J. Choi, and S. C. Jun, "A review of brain-computer interface games and an opinion survey from researchers, developers and users.," *Sensors (Basel).*, vol. 14, no. 8, pp. 14601–33, Aug. 2014.

[5] C. G. Coogan and B. He, "Brain-Computer Interface Control in a Virtual Reality

Environment and Applications for the Internet of Things," *IEEE Access*, vol. 6, pp. 10840–10849, 2018.

[6] K. LaFleur, K. Cassady, A. Doud, K. Shades, E. Rogin, and B. He, "Quadcopter control in three-dimensional space using a noninvasive motor imagery-based brain–computer interface," *J. Neural Eng.*, vol. 10, no. 4, p. 046003, Aug. 2013.

[7] S. Waldert, "Invasive vs. Non-Invasive Neuronal Signals for Brain-Machine Interfaces: Will One Prevail?," *Front. Neurosci.*, vol. 10, p. 295, 2016.

[8] F. Lotte, M. Congedo, A. Lécuyer, F. Lamarche, and B. Arnaldi, "A review of classification algorithms for EEG-based brain–computer interfaces," *J. Neural Eng.*, vol. 4, no. 2, pp. R1–R13, Jun. 2007.

[9] N. Weiskopf, K. Mathiak, S. W. Bock, F. Scharnowski, R. Veit, W. Grodd, R. Goebel, and N. Birbaumer, "Principles of a Brain-Computer Interface (BCI) Based on Real-Time Functional Magnetic Resonance Imaging (fMRI)," *IEEE Trans. Biomed. Eng.*, vol. 51, no. 6, pp. 966–970, Jun. 2004.

[10] S. Coyle, T. Ward, C. Markham, and G. McDarby, "On the suitability of near-infrared (NIR) systems for next-generation brain–computer interfaces," *Physiol. Meas.*, vol. 25, no. 4, pp. 815–822, Aug. 2004.

[11] J. R. Wolpaw, N. Birbaumer, D. J. McFarland, G. Pfurtscheller, and T. M. Vaughan, "Brain-computer interfaces for communication and control.," *Clin. Neurophysiol.*, vol. 113, no. 6, pp. 767–91, Jun. 2002.

[12] A. Y. Kaplan, A. A. Fingelkurts, A. A. Fingelkurts, S. V. Borisov, and B. S. Darkhovsky, "Nonstationary nature of the brain activity as revealed by EEG/MEG: Methodological, practical and conceptual challenges," *Signal Processing*, vol. 85, no. 11, pp. 2190–2212, Nov. 2005.

[13] S. Brandl, J. Hohne, K.-R. Muller, and W. Samek, "Bringing BCI into everyday life: Motor imagery in a pseudo realistic environment," in *2015 7th International IEEE/EMBS Conference on Neural Engineering (NER)*, 2015, pp. 224–227.

[14] M. Fatourechi, A. Bashashati, R. K. Ward, and G. E. Birch, "EMG and EOG artifacts in brain computer interface systems: A survey," *Clin. Neurophysiol.*, vol. 118, no. 3, pp. 480–494, Mar. 2007.

[15] N. Neumann and A. Kubler, "Training locked-in patients: a challenge for the use of

brain~computer interfaces," *IEEE Trans. Neural Syst. Rehabil. Eng.*, vol. 11, no. 2, pp. 169–172, Jun. 2003.

[16] K.-S. Hong and M. J. Khan, "Hybrid Brain–Computer Interface Techniques for Improved Classification Accuracy and Increased Number of Commands: A Review," *Front. Neurorobot.*, vol. 11, p. 35, Jul. 2017.

[17] R. Ramli, H. Arof, F. Ibrahim, N. Mokhtar, and M. Y. I. Idris, "Using finite state machine and a hybrid of EEG signal and EOG artifacts for an asynchronous wheelchair navigation," *Expert Syst. Appl.*, vol. 42, no. 5, pp. 2451–2463, Apr. 2015.

[18] H. Wang, Y. Li, J. Long, T. Yu, and Z. Gu, "An asynchronous wheelchair control by hybrid EEG–EOG brain–computer interface," *Cogn. Neurodyn.*, vol. 8, no. 5, pp. 399–409, Oct. 2014.

[19] K. Lin, A. Cinetto, Y. Wang, X. Chen, S. Gao, and X. Gao, "An online hybrid BCI system based on SSVEP and EMG," *J. Neural Eng.*, vol. 13, no. 2, p. 026020, Apr. 2016.

[20] M. Mano, A. Lécuyer, E. Bannier, L. Perronnet, S. Noorzadeh, and C. Barillot, "How to Build a Hybrid Neurofeedback Platform Combining EEG and fMRI.," *Front. Neurosci.*, vol. 11, p. 140, 2017.

[21] B. Koo, H.-G. Lee, Y. Nam, H. Kang, C. S. Koh, H.-C. Shin, and S. Choi, "A hybrid NIRS-EEG system for self-paced brain computer interface with online motor imagery," *J. Neurosci. Methods*, vol. 244, pp. 26–32, Apr. 2015.

[22] B. Z. Allison, E. W. Wolpaw, and J. R. Wolpaw, "Brain-computer interface systems: progress and prospects.," *Expert Rev. Med. Devices*, vol. 4, no. 4, pp. 463–74, Jul. 2007.

[23] P. V. Zephaniah and J. G. Kim, "Recent functional near infrared spectroscopy based brain computer interface systems: Developments, applications and challenges," *Biomed. Eng. Lett.*, vol. 4, no. 3, pp. 223–230, Sep. 2014.

[24] N. Naseer and K.-S. Hong, "fNIRS-based brain-computer interfaces: a review.," *Front. Hum. Neurosci.*, vol. 9, p. 3, 2015.

[25] A. Khalaf, M. Sybeldon, E. Sejdic, and M. Akcakaya, "A brain-computer interface based on functional transcranial doppler ultrasound using wavelet transform and support vector machines," *J. Neurosci. Methods*, vol. 293, pp. 174–182, Jan. 2018.

[26] B.-K. Min, M. J. Marzelli, and S.-S. Yoo, "Neuroimaging-based approaches in the brain–computer interface," *Trends Biotechnol.*, vol. 28, no. 11, pp. 552–560, Nov. 2010.

[27] A. Khalaf, E. Sejdic, and M. Akcakaya, “A novel motor imagery hybrid brain computer interface using EEG and functional transcranial Doppler ultrasound,” *J. Neurosci. Methods*, vol. 313, pp. 44–53, Feb. 2019.

[28] A. Khalaf, E. Sejdic, and M. Akcakaya, “Towards optimal visual presentation design for hybrid EEG—fTCD brain–computer interfaces,” *J. Neural Eng.*, vol. 15, no. 5, p. 056019, Oct. 2018.

[29] H. Ramoser, J. Muller-Gerking, and G. Pfurtscheller, “Optimal spatial filtering of single trial EEG during imagined hand movement,” *IEEE Trans. Rehabil. Eng.*, vol. 8, no. 4, pp. 441–446, 2000.

[30] A. V. Alexandrov, M. A. Sloan, L. K. S. Wong, C. Douville, A. Y. Razumovsky, W. J. Koroshetz, M. Kaps, and C. H. Tegeler, “Practice Standards for Transcranial Doppler Ultrasound: Part I-Test Performance,” *J. Neuroimaging*, vol. 17, no. 1, pp. 11–18, Jan. 2007.

[31] L. H. Monsein, A. Y. Razumovsky, S. J. Ackerman, H. J. W. Nauta, and D. F. Hanley, “Validation of transcranial Doppler ultrasound with a stereotactic neurosurgical technique,” *J. Neurosurg.*, vol. 82, no. 6, pp. 972–975, Jun. 1995.

[32] D. Devlaminck, B. Wyns, M. Grosse-Wentrup, G. Otte, and P. Santens, “Multisubject learning for common spatial patterns in motor-imagery BCI.,” *Comput. Intell. Neurosci.*, vol. 2011, p. 217987, Oct. 2011.

[33] Yijun Wang, Shangkai Gao, and Xiaornog Gao, “Common Spatial Pattern Method for Channel Selelction in Motor Imagery Based Brain-computer Interface,” in *2005 IEEE Engineering in Medicine and Biology 27th Annual Conference*, 2005, pp. 5392–5395.

[34] B. Blankertz, R. Tomioka, S. Lemm, M. Kawanabe, and K. Muller, “Optimizing Spatial filters for Robust EEG Single-Trial Analysis,” *IEEE Signal Process. Mag.*, vol. 25, no. 1, pp. 41–56, 2008.

[35] B. Blankertz, R. Tomioka, S. Lemm, M. Kawanabe, and K. Muller, “Optimizing Spatial filters for Robust EEG Single-Trial Analysis,” *IEEE Signal Process. Mag.*, vol. 25, no. 1, pp. 41–56, 2008.

[36] M. Grosse-Wentrup, C. Liefhold, K. Gramann, and M. Buss, “Beamforming in Noninvasive Brain–Computer Interfaces,” *IEEE Trans. Biomed. Eng.*, vol. 56, no. 4, pp. 1209–1219, Apr. 2009.

[37] Haiping Lu, How-Lung Eng, Cuntai Guan, K. N. Plataniotis, and A. N. Venetsanopoulos,

"Regularized Common Spatial Pattern With Aggregation for EEG Classification in Small-Sample Setting," *IEEE Trans. Biomed. Eng.*, vol. 57, no. 12, pp. 2936–2946, Dec. 2010.

[38] A. Khalaf, M. Sybeldon, E. Sejdic, and M. Akcakaya, "A brain-computer interface based on functional transcranial doppler ultrasound using wavelet transform and support vector machines," *J. Neurosci. Methods*, vol. 293, 2018.

[39] R. C. Blair and J. J. Higgins, "A Comparison of the Power of Wilcoxon's Rank-Sum Statistic to That of Student's t Statistic under Various Nonnormal Distributions," *J. Educ. Stat.*, vol. 5, no. 4, p. 309, 1980.

[40] C.-W. Chih-Wei Hsu and C.-J. Chih-Jen Lin, "A comparison of methods for multiclass support vector machines," *IEEE Trans. Neural Networks*, vol. 13, no. 2, pp. 415–425, Mar. 2002.

[41] B. Obermaier, C. Neuper, C. Guger, and G. Pfurtscheller, "Information transfer rate in a five-classes brain-computer interface," *IEEE Trans. Neural Syst. Rehabil. Eng.*, vol. 9, no. 3, pp. 283–288, 2001.

[42] M. J. Khan, M. J. Hong, and K.-S. Hong, "Decoding of four movement directions using hybrid NIRS-EEG brain-computer interface," *Front. Hum. Neurosci.*, vol. 8, p. 244, Apr. 2014.

[43] F. Putze, S. Hesslinger, C.-Y. Tse, Y. Huang, C. Herff, C. Guan, and T. Schultz, "Hybrid fNIRS-EEG based classification of auditory and visual perception processes.," *Front. Neurosci.*, vol. 8, p. 373, 2014.

[44] A. P. Buccino, H. O. Keles, and A. Omurtag, "Hybrid EEG-fNIRS Asynchronous Brain-Computer Interface for Multiple Motor Tasks," *PLoS One*, vol. 11, no. 1, p. e0146610, Jan. 2016.

[45] S. Fazli, J. Mehnert, J. Steinbrink, G. Curio, A. Villringer, K.-R. Müller, and B. Blankertz, "Enhanced performance by a hybrid NIRS–EEG brain computer interface," *Neuroimage*, vol. 59, no. 1, pp. 519–529, Jan. 2012.

[46] Y. Blokland, L. Spyrou, D. Thijssen, T. Eijsvogels, W. Colier, M. Floor-Westerdijk, R. Vlek, J. Bruhn, and J. Farquhar, "Combined EEG-fNIRS Decoding of Motor Attempt and Imagery for Brain Switch Control: An Offline Study in Patients With Tetraplegia," *IEEE Trans. Neural Syst. Rehabil. Eng.*, vol. 22, no. 2, pp. 222–229, Mar. 2014.

[47] X. Yin, B. Xu, C. Jiang, Y. Fu, Z. Wang, H. Li, and G. Shi, "A hybrid BCI based on EEG

and fNIRS signals improves the performance of decoding motor imagery of both force and speed of hand clenching," *J. Neural Eng.*, vol. 12, no. 3, p. 036004, Jun. 2015.

[48] J. Shin, K.-R. Müller, C. H. Schmitz, D.-W. Kim, and H.-J. Hwang, "Evaluation of a Compact Hybrid Brain-Computer Interface System," *Biomed Res. Int.*, vol. 2017, pp. 1–11, Mar. 2017.